SUPPLEMENTARY INFORMATION

MATERIALS & METHODS

Immunohistochemistry. Sections of formalin-fixed paraffin-embedded tissue specimens were stained with monoclonal mouse anti-human CD3 (clone F7.2.38; dilution 1:50; DAKO Cytokeratin, Glostrup, Denmark), monoclonal mouse anti-human CD8 (clone C8/144B; dilution 1:30; DAKO Cytokeratin), monoclonal mouse anti-human CD4 (clone 4B12; dilution 1:20; Labvision, Fremont, USA), rabbit anti-human/mouse caspase 3 Active (clone AF835; dilution 1:25; R&D Systems) and FOXP3 (clone 236A/E7; dilution 1:500; Abcam), Pan-ZK (clone MNF116; dilution 1:100; DAKO Cytokeratin), Ki-67 (clone MIB-1, ready-to-use, DAKO OMNIS), CMV (clone CCH2 + DDG9; dilution 1:50; DAKO Cytokeratin), Adenovirus (clone 20/11, dilution 1:50; Chemicon) as recommended by the suppliers.

DNA extraction & 16S rRNA gene PCR. Stool samples and mucosal biopsies obtained at endoscopy were immediately frozen and stored at -20°C. DNA extraction from stool samples and biopsies was performed by mechanical lysis with a MagnaLyser Instrument (Roche Diagnostics, Mannheim, Germany) and subsequent total bacterial genomic DNA isolation with the MagNA Pure LC DNA Isolation Kit III (bacteria, fungi) in a MagNA Pure LC 2.0 Instrument (Roche Diagnostics) according to the manufacturer's instructions. For amplification of the bacterial 16S rRNA gene FLX one-way fusion primer (Lib-L kit, Primer A, Primer B; Roche 454 Life Science, Branford, CT) with the template-specific sequence F27— AGAGTTTGATCCTGGCTCAG and R357— CTGCTGCCTYCCGTA targeting the hypervariable regions V1 and V2 were used. PCR reactions for each sample were performed in triplicates. Subsequently the amplicons were purified according to standard procedures, quantified, pooled and sequenced with the GS FLX Titanium Sequencing Kit XLR70 (Roche 454 Life Science, Branford, CT, USA) according to manufacturer's instructions. 16S rRNA gene pyrosequencing data has been deposited in EBI-SRA under the accession number ERP013256. Sample set information is given in table S6.

Microbiota analysis. Raw files from 454 FLX pyrosequencing were processed with MOTHUR v. 1.31.2 according to the standard 454 SOP of MOTHUR (1)**.** Sequencing errors were reduced using mothur's implementation of PyroNoise (2), and the command pre.cluster (3) was used to remove sequences that arose due to pyrosequencing errors. Chimeras were removed with UCHIME (4) and non-bacterial contaminants as chloroplasts and mitochondria were removed using the Ribosomal Database Project (RDP) reference (5). The high quality reads were aligned to the SILVA database (6, 7). For an OTU based analysis, the processed fasta files from mothur were introduced into QIIME version 1.7.0 (8). Command pick_de_novo_otus.py was used for OTU picking, OTU were formed by clustering with uclust (similarity score of 97%) and taxonomy was assigned using the RDP-classifier (version 2.2, confidence threshold of 0.8) and Greengenes reference (gg_12_10). The biom file was further analysed with the command core_diversity.py. For this analysis the samples were rarefied to 750 sequences/sample. For single OTUs a standard NCBI nucleotide BLAST with the "16S ribosomal RNA sequences (Bacteria and Archaea)" database was performed. Groups and categories for analysis of the sample set are listed in Table S4. P-values below 0,05 were considered statistically significant ($P<0.05$=*; $P<0.01$=**; $P<0.001$=***). Presented values are always mean ± SEM if not indicated otherwise.

qPCR analysis of butyrate producing genes and bacterial load. Quantitative analysis of microbial butyrate kinase (*buk*) and butyryl-CoA:acetate CoA-transferase (*but*) genes in stool samples was performed according to Vital et al. (9). qPCR was performed with the Power SYBR® Green Mix (Applied Biosystems) on a LightCycler® 480 instrument (Roche Life Science) according to the suppliers recommendations; the following oligonucleotide primers were used: buk - G_buk_F/R (*Clostridium acetobutylicum, C. butyricum, C. perfringens*); but - G_Acida_F/R (*Acidaminococcus* sp.), G_Fprsn_F/R (*Faecalibacterium prausnitzii*), G_RosEub_F/G_Ros_R/G_Eub_R (*Roseburia* sp., *Eubacterium rectale*) (9); 16S rDNA - 1132F/1108R (universal) (10).

For the determination of bacterial load in stool samples, DNA was isolated from 250 mg stool samples with the PowerLyzer® PowerSoil® DNA Isolation Kit (MoBio). The 16S rDNA was quantified in 3µl of the DNA eluate by qPCR (oligonucleotide primers 1132F/1108R; 10) and the signal was correlated to a

standard curve of genomic DNA from *E. coli* DH5α with given concentrations. The results were adjusted to 1g of total stool.

Short-chain fatty acid measurements by GC-MS. Acetate, propionate and butyrate levels from stool samples were measured by GC-MS using a Thermo Scientific DSQ II™ Series Single Quadrupole GC-MS by electron ionization instrument. 500µl stool homogenizate were mixed with 500µl H_3PO_4 (0.5%), internal standards (ISTD: 200µl dC2 [500µM] and 200µl dC4 [500µM]) and 600µl methyl *tert*-butyl ether (MTBE). After centrifugation (10 min; 2.500 rpm; RT) 150µl of the organic phase was used for the measurement. A calibration curve was created with increasing ISTDs mixed with H_3PO_4 (0,5%) for the analysis.

References

1) Schloss PD, Gevers D, Westcott SL. Reducing the effects of PCR amplification and sequencing artifacts on 16S rRNA-based studies. PLoS One 2011; 6: e27310.

2) Quince C, Lanzén A, Curtis TP, et al. Accurate determination of microbial diversity from 454 pyrosequencing data. Nat Methods 2009; 6: 639–41.

3) Huse SM, Welch DM, Morrison HG, et al. Ironing out the wrinkles in the rare biosphere through improved OTU clustering. Environ Microbiol 2010; 12: 1889– 98.

4) Edgar RC, Haas BJ, Clemente JC, et al. UCHIME improves sensitivity and speed of chimera detection. Bioinformatics 2011; 27: 2194–200.

5) Wang Q, Garrity GM, Tiedje JM, et al. Naive Bayesian classifier for rapid assignment of rRNA sequences into the new bacterial taxonomy. Appl Environ Microbiol 2007; 73: 5261–7.

6) Quast C, Pruesse E, Yilmaz P, et al. The SILVA ribosomal RNA gene database project: improved data processing and web-based tools. Nucleic Acids Res 2013; 41: D590–596.

7) Pruesse E, Quast C, Knittel K, et al. SILVA: a comprehensive online resource for quality checked and aligned ribosomal RNA sequence data compatible with ARB. Nucleic Acids Res 2007; 35: 7188–96.

8) Caporaso JG, Kuczynski J, Stombaugh J, et al. QIIME allows analysis of high-throughput community sequencing data. Nat Methods 2010; 7: 335–6.

9) Vital M, Penton CR, Wang Q, et al. A gene-targeted approach to investigate the intestinal butyrate-producing bacterial community. Microbiome 2013, 1:8

10) Leigh MB, Pellizari VH, Uhlík O, et al. Biphenyl-utilizing bacteria and their functional genes in a pine root zone contaminated with polychlorinated biphenyls (PCBs). ISME J 2007, 1:134-148.

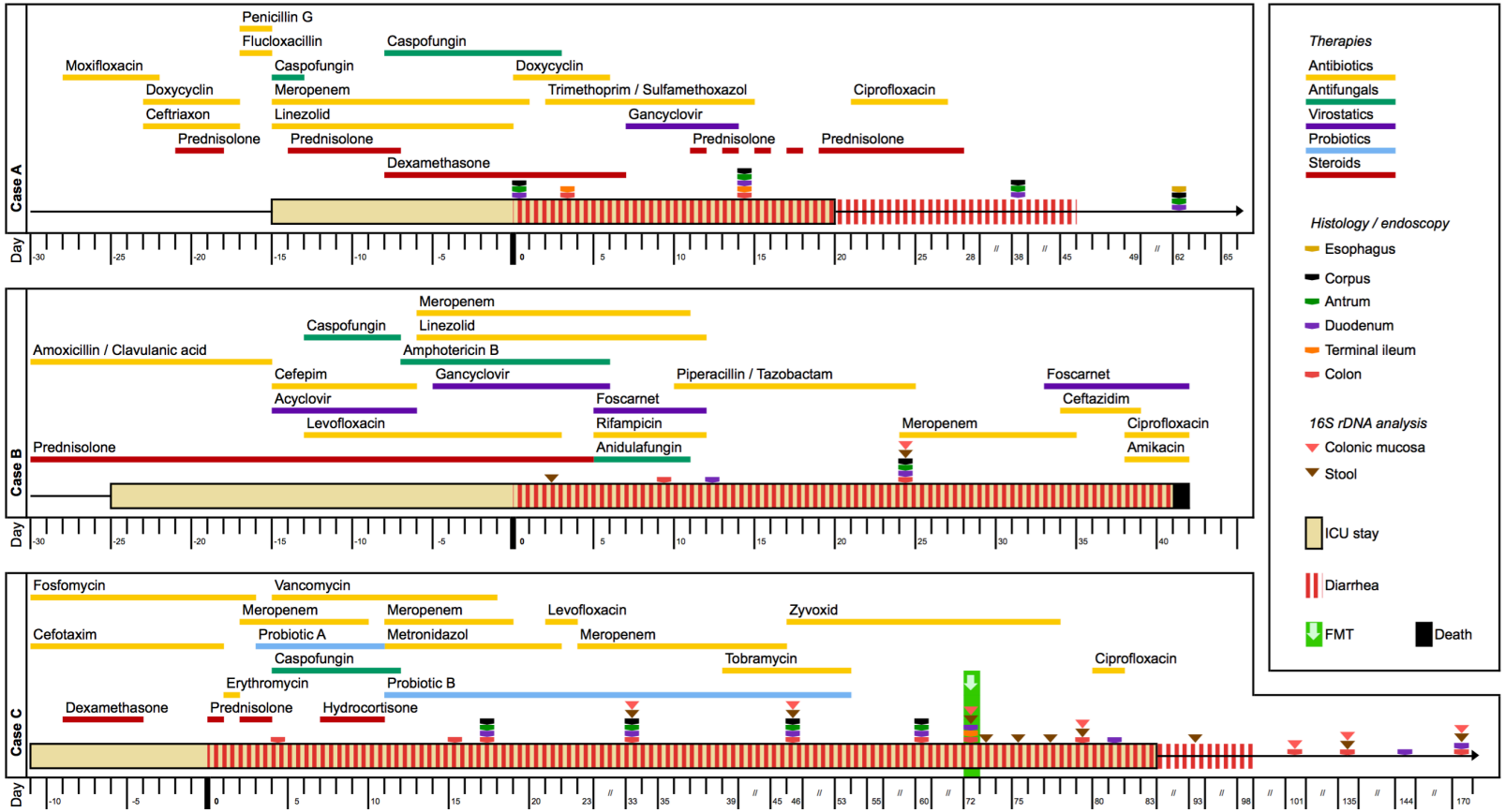

Figure S1. Clinical courses of patients. Admission to the ICU and duration of diarrhea are indicated as boxes at the bottom of each case. Days are counted in relation to diarrhea onset. Therapies including antibiotics, antifungals, virostatics, steroids as well as probiotics are indicated together with endoscopic examinations and samples obtained for histology and microbiota analyses (probiotic A: *Saccharomyces boulardii*; probiotic B: *Lactobacillus acidophilus, L. paracasei, L. rhamnosus, L. salivarius, L. plantarum, Enterococcus faecium, Bifidobacterium bifidum, B. lactis, B. longum*).

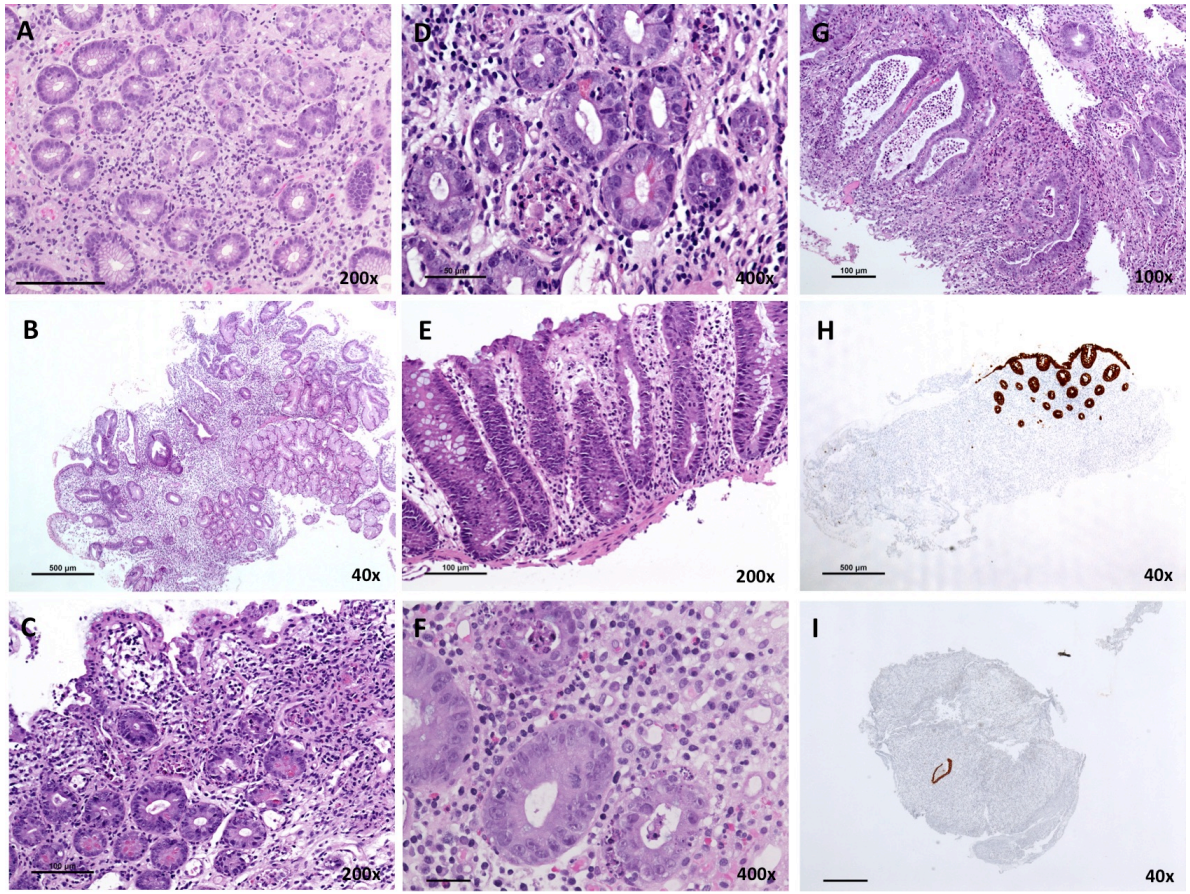

Figure S2. Histological features. (A) Focally enhanced mild chronic active gastritis (case C, day 33); **(B)** Duodenal villus blunting and crypt loss (case C, day 17); **(C, D)** Villus blunting, crypt loss and abundant apoptosis in the ileal mucosa (case A, day 3); **(E)** Abundant colonic crypt apoptosis (case A, day 3); **(F)** Abundant colonic crypt apoptosis (case C, day 15); **(G)** Neutrophilic granulocytes intermixed with cell debris in crypts (case C, day 17); **(H, I)** Denuded colonic mucosa, remnant crypt epithelium stained with anti-panzytokeratin antibody (case C, day 4 and day 33, respectively).

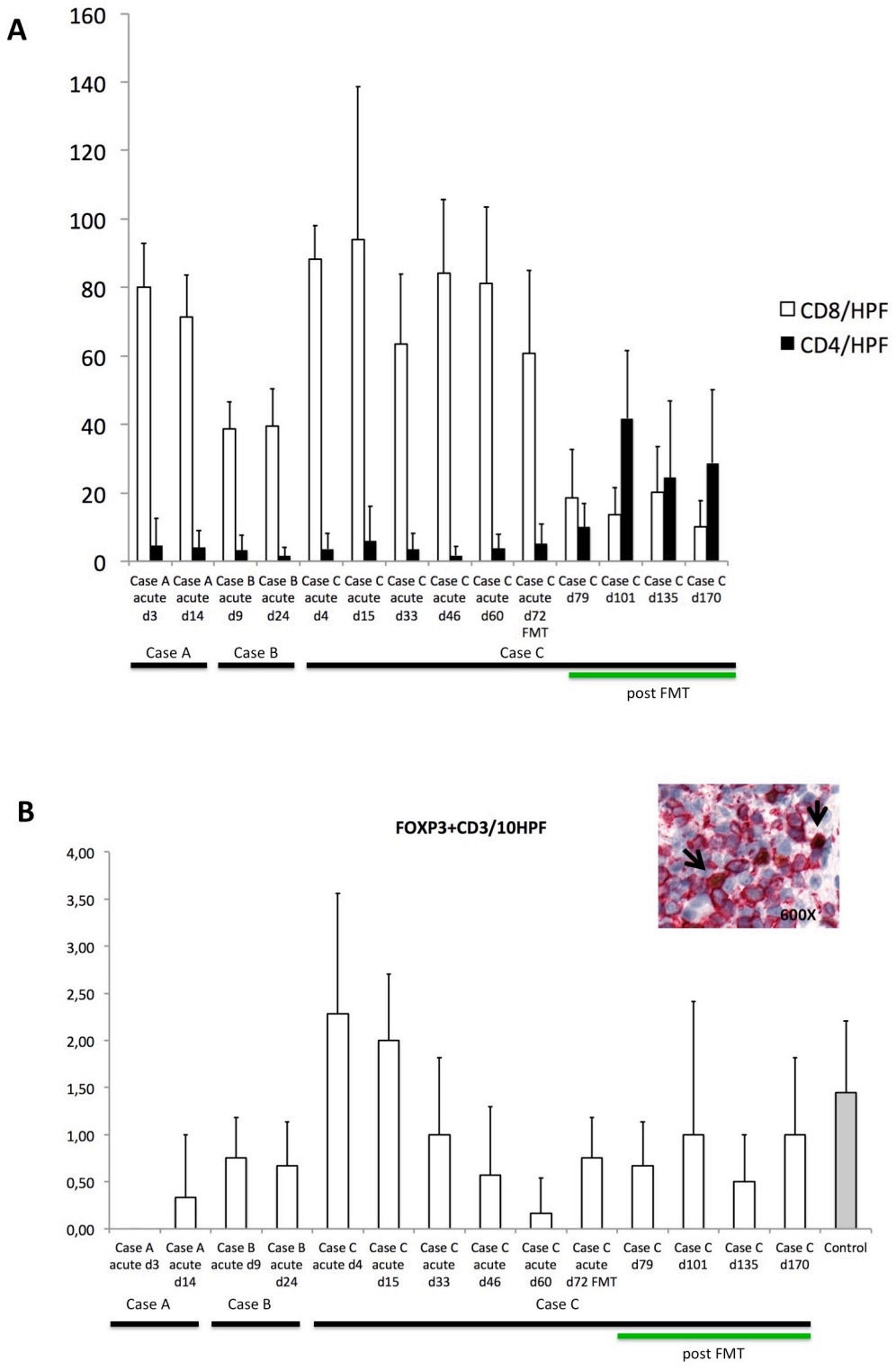

Figure. S3. (A) $CD8^+$ and $CD4^+$ T lymphocyte counts in the colonic mucosa of patients with AAA enterocolitis assessed by immunohistochemistry (scored per high-power field, HPF). **(B)** Regulatory T cell counts assessed by double-immunostaining of the markers FOXP3 und CD3 (scored per 10 HPF). Representative picture (inset) of membranous CD3 positivity (red) and nuclear FOXP3 positivity (brown). Double marked cells are indicated with arrows. Days (d) are counted from the onset of diarrhea.

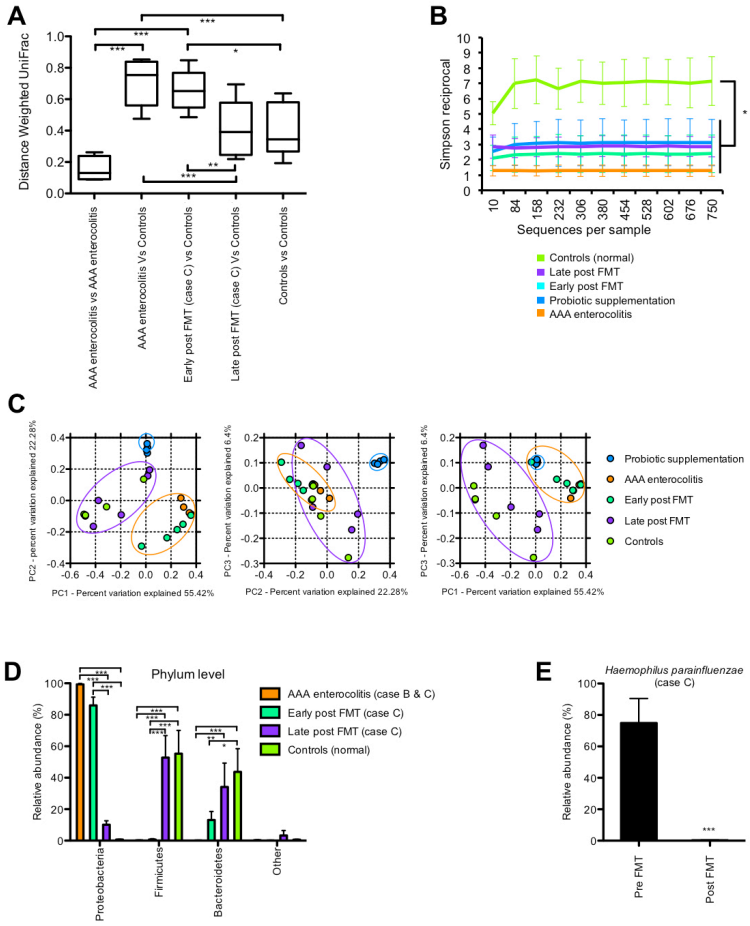

Figure S4. Microbiota dynamics and the effect of FMT in AAA enterocolitis. (A) Comparison of weighted UniFrac distances from stool and colonic mucosa samples of cases B and C at acute phase of disease indicates a more similar microbiota composition of cases when compared to controls. After FMT distances significantly decrease indicating that post transplantation the microbiota of case C approaches towards a normal stool microbiota (note: a low distance value indicates a more similar microbiota composition between assessed samples; two-way ANOVA, Bonferroni post-test; *p<0,05, ** p<0,01, *** p<0,001). **(B)** Microbiota diversity displayed with the Simpson reciprocal metric. Diversity is highly reduced in AAA enterocolitis and gradually increased during probiotic supplementation and after FMT, although control samples show a significantly higher diversity compared to all other groups (two-sample t-test using 999 Monte Carlo permutations and Bonferroni correction; p<0.05). **(C)** PCoA plots based on weighted UniFrac distances show a significant grouping of samples originating stool samples from the acute phase of cases B and C together with samples early after FMT from case C. Samples originating from later phases after FMT (latepostFMT: from day 21d post FMT) group together with control samples indicating a reestablishment of a normal microbiota. Samples originating from the probiotic treatment during acute disease of case C group individually (ANOSIM; p<0.001). **(D)** Proteobacteria are dominating in AAA enterocolitis and phylum wide microbiota changes due to FMT (sample designations are given in Tab. S4; two-way ANOVA, Bonferroni post-test; *p<0,05, ** p<0,01, *** p<0,001). **(E)** Opportunistic *H. parainfluenzae* completely diminishes after FMT in mucosa and stool samples of case C (pre FMT: n=2; post FMT n=11; ANOVA, Bonferroni- and FDR-corrected; *** p<0,001).

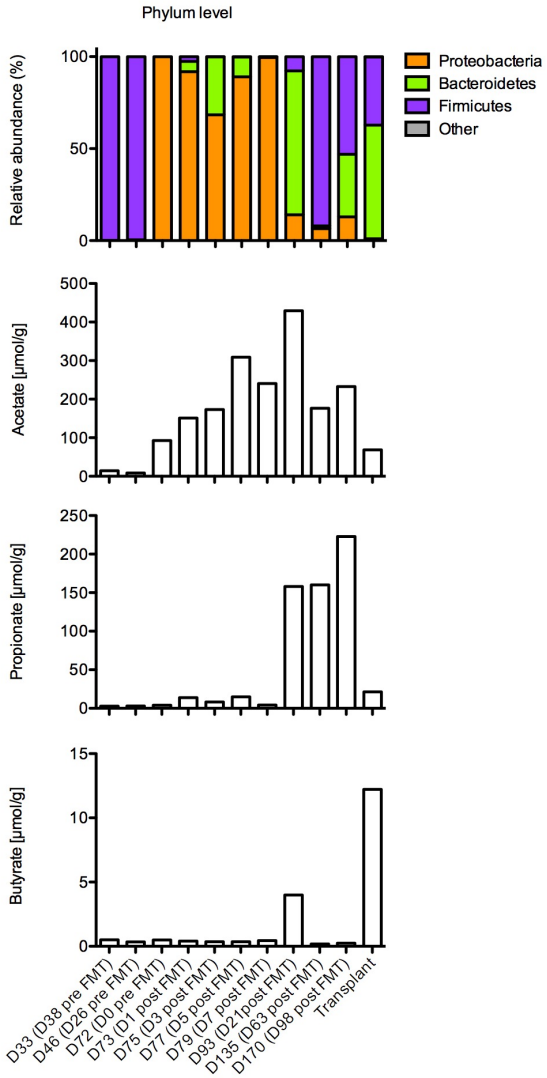

Figure S5. Short-chain-fatty-acid levels in stools of case C. GC/MS analyses SCFAs in case C pre and post FMT compared to the transplant. SCFAs are broadly decreased during the acute phase. A prominent increase of acetate levels in stools, correlating with the recolonization of Bacteroidetes, and an increase of propionate levels during recolonization of Firmicutes could be detected directly after FMT. No significant increase of butyrate levels was noted. The lack of butyrate post FMT might be due to low-level colonization of typical butyrate producers like members of the families *Lachnospiraceae* and *Ruminococcaceae* (0-7% abundance); at D93 3,99 µmol/g butyrate was measurable correlating with 7% *Lachnospiraceae* and *Ruminococcaceae*). The transplant shows elevated butyrate levels and a relative abundance of 33% of these well-known butyrate producers.

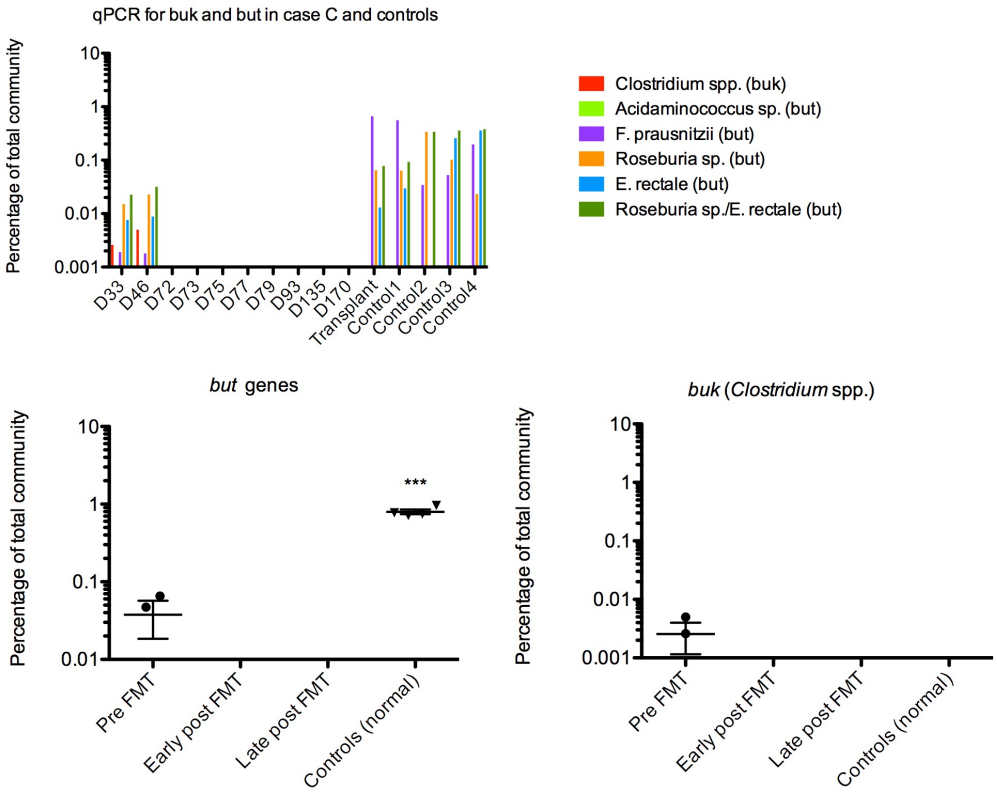

Figure S6. Butyrate producing genes in fecal specimens of case C. Quantitative PCR of *but* genes compared to total 16S RNA genes shows a significant increase in control stools compared to stools from case C pre and post FMT (One-way ANOVA, *** $p<0.0001$; note: positive samples for *but* pre FMT were taken during probiotic treatment). No significant difference between groups could be measured for *buk* genes. These results correlate with the GC/MS data showing no increase of butyrate in feces of patient C post FMT.

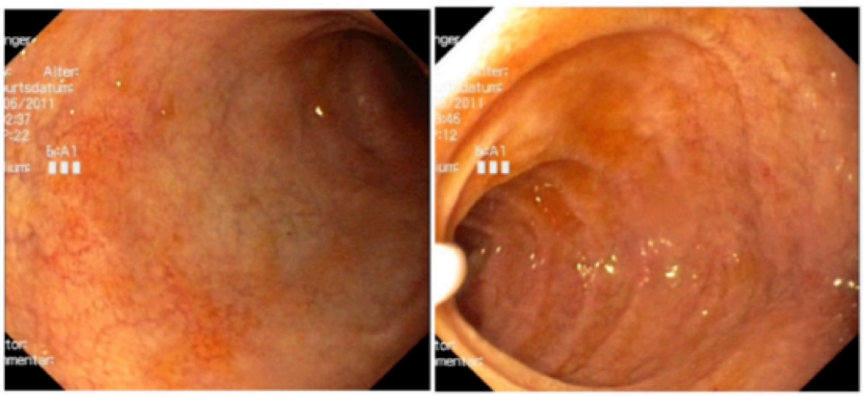

Figure S7. Endoscopic appearance 97 days post FMT in case C. Only a discrete mucosal hyperemia is visible in the colonic (upper left) and duodenal mucosa (upper right).